Title

Irreversible electroporation ablation overcomes tumor-associated immunosuppression to improve the efficacy of DC vaccination in a mice model of pancreatic cancer

Journal

OncoImmunology, 10(1)

ISSN

2162-4011

Authors

Yang, Jia
Eresen, Aydin
Shangguan, Junjie
et al.

Publication Date

2021

DOI

10.1080/2162402x.2021.1875638

Peer reviewed

ONCOIMMUNOLOGY
2021, VOL. 10, NO. 1, e1875638 (9 pages)
https://doi.org/10.1080/2162402X.2021.1875638

Taylor & Francis
Taylor & Francis Group

ORIGINAL RESEARCH

OPEN ACCESS Check for updates

Irreversible electroporation ablation overcomes tumor-associated immunosuppression to improve the efficacy of DC vaccination in a mice model of pancreatic cancer

Jia Yang[a], Aydin Eresen[a], Junjie Shangguan[a], Quanhong Ma[a], Vahid Yaghmai[a,b], and Zhuoli Zhang[a,b,c]

[a]Department of Radiology, Feinberg School of Medicine, Northwestern University, Chicago, IL, USA; [b]Department of Radiological Sciences, School of Medicine, University of California, Irvine, CA, USA; [c]Chao Family Comprehensive Cancer Center, University of California, Irvine, CA, USA

ABSTRACT

Pancreatic ductal adenocarcinoma (PDAC) is associated with highly immunosuppressive tumor microenvironment (TME) that can limit the efficacy of dendritic cell (DC) vaccine immunotherapy. Irreversible electroporation (IRE) is a local ablation approach. Herein, we test the hypothesis that IRE ablation can overcome TME immunosuppression to improve the efficacy of DC vaccination using *Kras*$^{LSL\text{-}G12D}$-*p53*$^{LSL\text{-}R172H}$-*Pdx-1-Cre* (KPC) orthotopic mouse model of PDAC. The median survival for mice treated with the combined IRE and DC vaccination was 77 days compared with sham control (35 days), DC vaccination (49 days), and IRE (44 days) groups (P = .006). Thirty-six percent of the mice treated with combination IRE and DC vaccination were still survival at the end of the study period (90 days) without visible tumor. The changes of tumor apparent diffusion coefficient (ΔADC) were higher in mice treated with combination IRE and DC vaccination than that of other groups (all P < .001); tumor ΔADC value positively correlated with tumor fibrosis fraction (R = 0.707, P < .001). IRE induced immunogenic cell death and alleviation of immunosuppressive components in PDAC TME when combined with DC vaccination, including increased tumor infiltration of $CD8^+$ T cells and Granzyme B^+ cells (P = .001, and P = .007, respectively). Our data show that IRE ablation can overcome TME immunosuppression to improve the efficacy of DC vaccination in PDAC. Combination IRE ablation and DC vaccination may enhance therapeutic efficacy for PDAC.

ARTICLE HISTORY
Received 21 October 2020
Revised 7 January 2021
Accepted 8 January 2021

KEYWORDS
Irreversible electroporation; dendritic cell vaccine; pancreatic ductal adenocarcinoma; magnetic resonance imaging

Introduction

Pancreatic ductal adenocarcinoma (PDAC) is one of the most aggressive neoplastic diseases with no effective treatment and with one of the lowest survival rates of any cancer.[1] As PDAC is mostly diagnosed at advanced stages, only 20% of the patients have resectable tumors and 60% of the patients who undergo surgical resection subsequently relapse.[2] This highlights the urgent need for the development of novel therapeutic approaches such as immunotherapy in PDAC.

Immunotherapy regulates the patient's immune response to tumor-associated antigens (TAAs), eliminates cancer cells by reducing patient tolerance to TAAs and inducing endogenous antitumor immunity, and provides long-term protection against cancer. Dendritic cell (DC) based therapy is a potent immunotherapeutic approach,[3,4] which has been recently used in clinical trials for various cancers, including PDAC. However, to date, DC immunotherapy has only provided limited clinical benefit in PDAC patients due to the particularly immunosuppressive tumor microenvironment (TME) which restricts the infiltration and function of T cells.

Irreversible electroporation (IRE) ablation is a nonthermal technique that involves targeted delivery of short pulses of strong electric fields to induce tissue death by means of cell membrane permeabilization.[5] Recently, IRE has been used for the local ablation of advanced/unresectable PDAC in both preclinical and clinical settings.[6–9] Several studies have demonstrated that IRE induces a powerful antitumor immune response that leads to tumor regression via destruction of TME, induction of tumor cell apoptosis, and activation of antigen-presenting cells.[10,11] Recent studies demonstrated that IRE ablation increases the total population of NK1.1 cells, $CD8^+$ T cells, $CD11c^+$ DCs, and $F4/80^+$ inflammatory monocyte cells in both blood and tumor of PDAC mouse models and showed that IRE invokes a systemic immune response.[12–14] IRE also destroys tumor fibrosis resulting tumor tissue permeability[12–14] which facilitates the migration of activated cytotoxic T lymphocytes to migrate into tumor tissue for immunotherapy. Therefore, both primary tumor ablation and systemic antitumor immune response induced by IRE ablation may overcome the immunosuppressive TME associated with DC-vaccine therapy. However, the potential for combining IRE with DC vaccination remains undefined.

Magnetic resonance imaging (MRI) is one of the most important tools for noninvasively monitoring pancreatic tumor burden for both disease progression and treatment response.[15,16] Diffusion-weighted MRI (DW-MRI) has showed to be very sensitive for the detection of tissue damage and cell death induced by IRE.[17] The purpose of this study was to evaluate whether 1) IRE ablation overcomes TME immunosuppression to improve the efficacy of DC vaccination and 2) DW-MRI biomarker, apparent diffusion coefficient (ADC), has a potential to capture tumor histological changes after IRE ablation.

CONTACT Zhuoli Zhang Email zhuoliz1@hs.uci.edu Department of Radiological Science, Co-Director of In-Vivo Functional Onco-Imaging Shared Resource, Director of Translational Imaging Lab, Chao Family Comprehensive Cancer Center, University of California, Irvine, CA 92617, USA.

Results

In vivo antitumor effect of IRE in combination with DC vaccine in pancreatic cancer

We first examined the antitumor efficacy of DC vaccination and IRE in the KPC mice model. The experimental set up, MRI scanning and treatment schedule are depicted in Figure 1(a). We observed a median survival of 35 days for untreated control group, 49 days for DC vaccination group, and 44 days for mice treated with IRE. Nevertheless, the median survival time for mice treated with the combined IRE with DC vaccination was 77 days, which is significantly improved than those in the other groups ($P < .01$, log-rank test). Meanwhile, five of the eleven (36%) mice in the combined IRE with DC vaccination group were still alive at the end of the study period (90 days) without visible tumor (Figure 1(b)).

In vitro cytotoxicity assays of IRE in KPC cells

Next, we investigated the cell death mode induced by IRE in KPC cells by *in vitro* study. Compared to the untreated cells, IRE-treated KPC cells were significantly increased in the Annexin V^+/PI^+ cells (Figure 2(a)). In addition, the cell viability was less than 1% when high voltage (1000 V) was applied, suggesting a rapid induction of late apoptosis and necrosis. We also analyzed the level of adenosine triphosphate (ATP), one of the validated the pathogen-associated molecular patterns, in supernatants of IRE-treated cells. IRE at 500 V and 1000 V caused a significantly increased level of extracellular ATP in the KPC cells (Figure 2(b)). In contrast, pulse at a high voltage of KPC cells showed no significant increase in the concentration of ATP, which may be due to most of the cells were rapidly dying.

In vivo effects of the combination of IRE and DC vaccination on tumor necrosis and apoptosis

All mice were euthanized after the last MRI examination for histologic examinations. We observed higher percentages of the necrotic area in the treated tumors, particularly treated with IRE with DC vaccination, compared with untreated tumors in H&E stained slices (Figure 3(a)). Therefore, by combining IRE with DC vaccines, an additive effect was evoked that enhanced the KPC tumor ablation area. Meanwhile, KPC tumor samples underwent CK19 staining to assess the ductal marker expression after different treatments. As shown in Figure 3(b) and Figure 3(d), no significant changes of the CK19 positive ductal area were observed between different

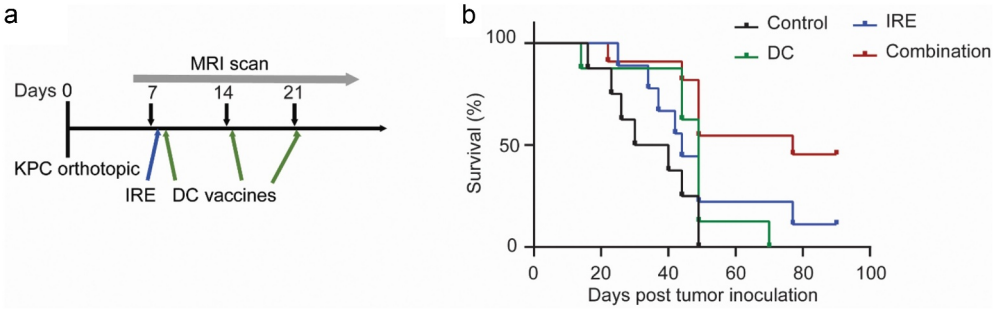

Figure 1. KPC mice survival after treatment with IRE and/or DC vaccines. (a), Treatment schedule. C57BL/6 mice bearing orthotopic KPC tumors were enrolled for treatment one week after the tumor cells inoculation. Sham surgery was performed on both control and DC vaccination treatment groups. (b), Kaplan–Meier survival analysis of mice with KPC tumors treated with sham control (n = 8), IRE (n = 9), DC vaccine (n = 8), or IRE + DC vaccine (n = 11). $P = .006$, log-rank test.

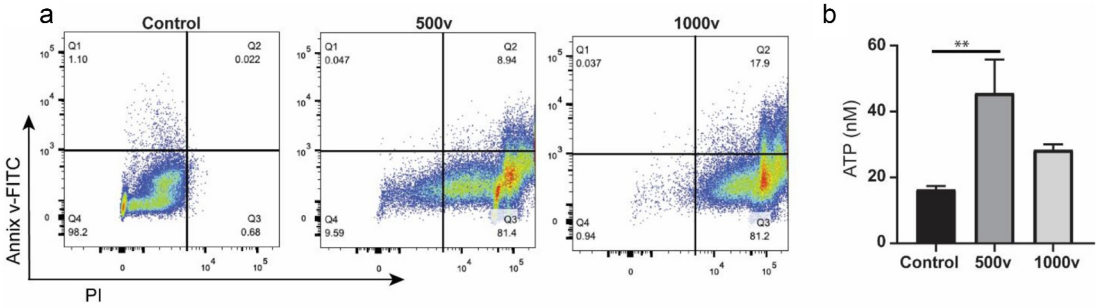

Figure 2. In vitro analyses of IRE-treated KPC cells. (a), Annexin V-FITC/PI staining of KPC cells. Cells were suspended in phosphate-buffered saline (PBS) and electroporated in a cuvette with a 4-mm gap. The parameters for electroporation were voltage = 500 or 1000 V, pulse duration = 100 μs, pulse repetition frequency = 1 Hz, number of pulses = 20. Cells were stained and analyzed within 30 min of treatment. (b), ATP concentrations in cell supernatants of untreated control, 500 V, and 1000 V groups. Data are presented as mean ± standard error of mean (SEM), n = 5. ** $P = .009$.

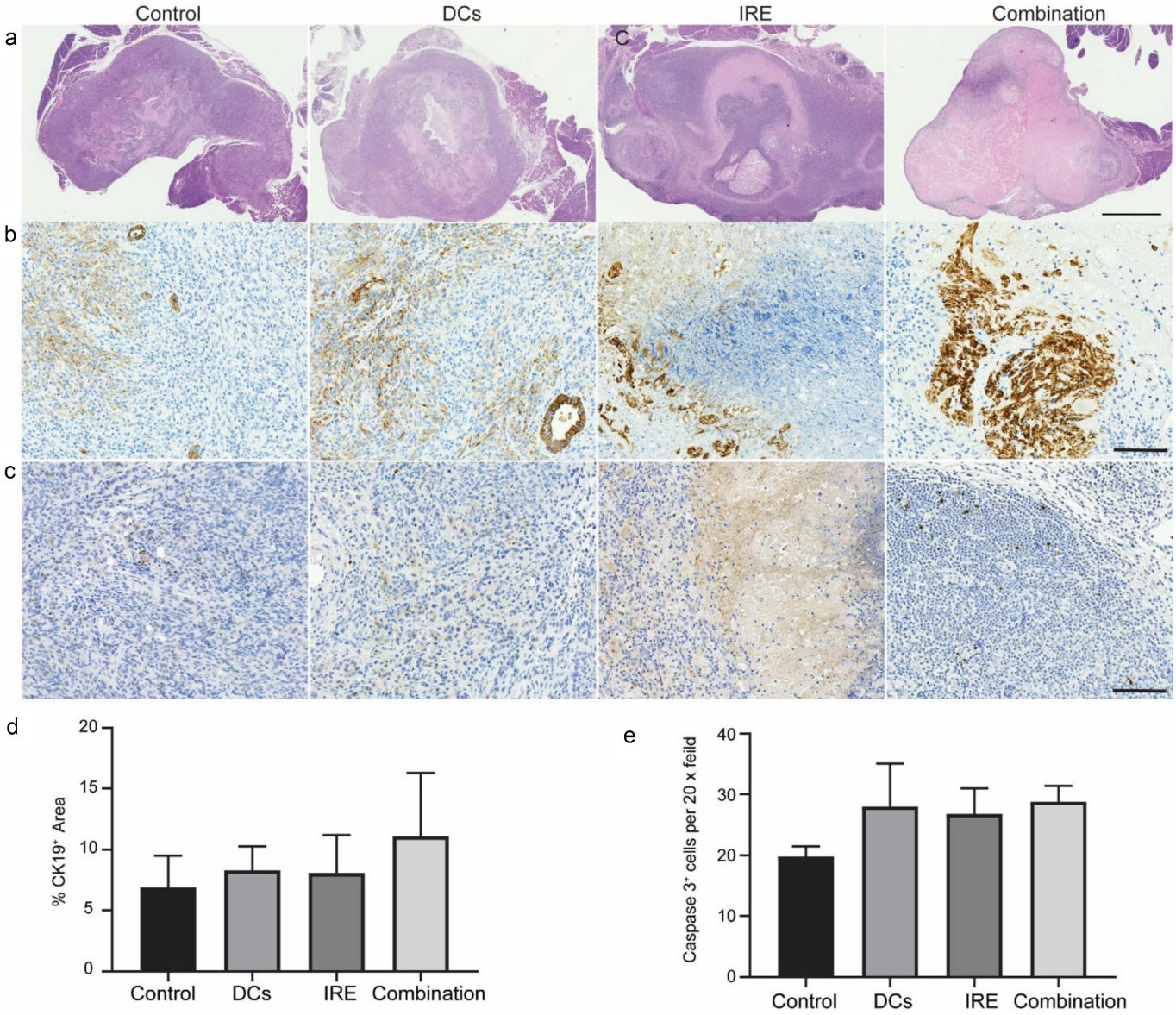

Figure 3. Comparison of tissue sections with H&E staining in (a), CK19 staining in (b), and cleaved caspase 3 staining in (c), three weeks after tumor inoculation in different groups. Scale bars in A represent 1.5 mm. Scale bars in (b)and (c)represent 100 µm. Relative quantification of $CK19^+$ area (d) and cleaved caspase 3^+ cells (e) in KPC tumors for each group. Data are presented as mean ± SEM, n = 5.

groups. Additionally, the induction of apoptosis after treatment was assessed by cleaved caspase 3 immunostaining which was not significantly different between groups (Figure 3(c) and Figure 3(e)).

MRI of KPC tumor

We monitored the tumor growth after different treatments with another 20 KPC tumor-bearing mice (5 mice per group) in a separate study by MRI. Representative T2W images of pancreatic tumors at different time points are shown from the same mouse in Figure 4(a). All pancreatic tumors were detectable on MRI by 1-week post-tumor inoculation regardless of the treatment approach and were increased in size with time. There was no statistically significant difference in the tumor growth rate between different groups in the first 3 weeks (all $P > .05$).

The mean baseline ADC values among all the KPC tumors were 0.74×10^{-3} $mm^2/s \pm 0.024$ for control group, 0.78×10^{-3} $mm^2/s \pm 0.078$ for DC vaccine group, 0.71×10^{-3} $mm^2/s \pm 0.017$ for IRE treatment group, and 0.73×10^{-3} $mm^2/s \pm 0.045$ for combination treatment group (Figure 4(b) and Figure 4(c)). After treatment, IRE-treated and combined IRE with DC vaccination treated tumor showed increased ADC values (Figure 4(b)). There was no statistical difference in ADC values between different groups at different time points ($P = .21$; Figure 4(c)). Although ΔADC_{3w} in combined IRE with DC vaccination was higher than other groups, this did not reach statistical significance ($P = .075$, data not shown). However, ΔADC_{2w} was significantly higher in combined IRE with DC vaccination treated tumors than in control tumors ($P < .001$; Figure 4(d)). Meanwhile, we evaluated the fraction of fibrotic area per pancreas based on trichrome staining. There

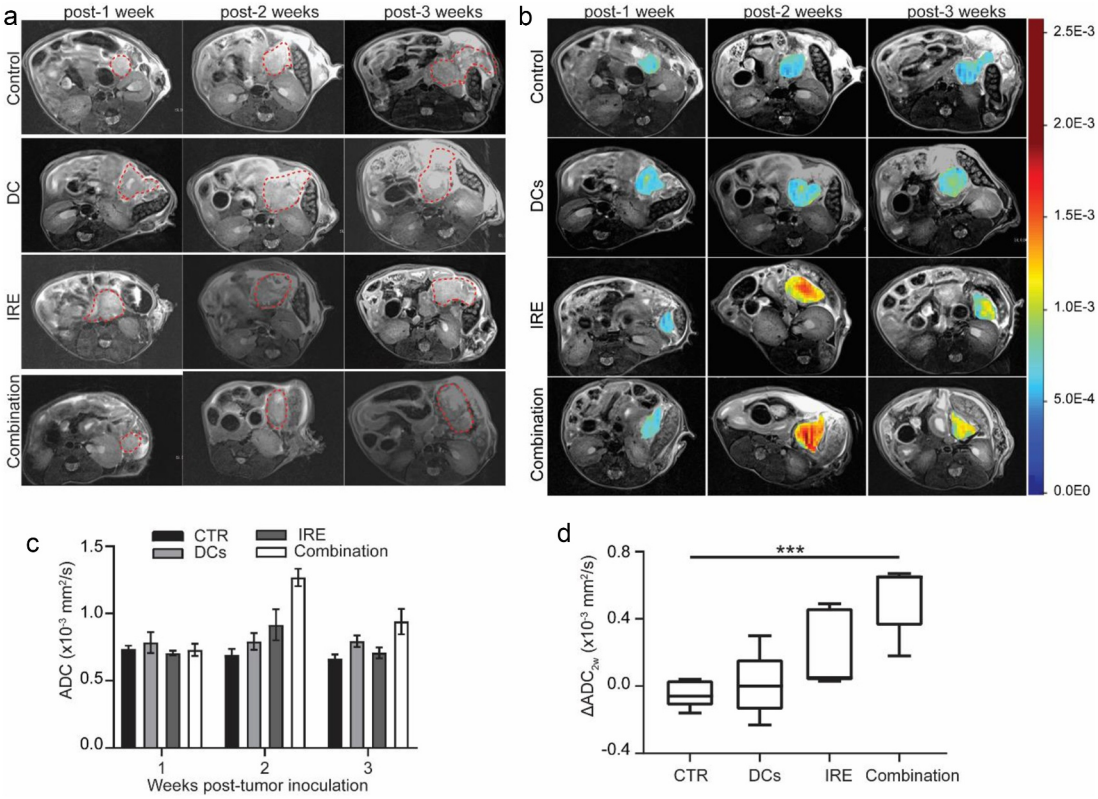

Figure 4. T2W images, diffusion-weighted images and analyses. (a), Representative T2W images of a KPC tumor-bearing mouse from each group in a separate study. MRI slices with the largest tumor cross-section are presented to show tumor size at each time point. Red contour denotes area of pancreatic tumor. (b), Representative ADC pseudocolor maps of the tumor overlaid onto a T2W image from KPC mice in different groups are shown. (c), Changes in ADC values (ΔADC_{2w}) of KPC tumor in different groups at different time points. data are presented as mean ± SEM, n = 5. (d), Box plot shows a statistically significant difference in ΔADC between combination IRE with DC vaccine group and control KPC tumors. ***$P < .001$.

was no significant difference in collagen deposition in different groups at 3 weeks (Figure 5(a-d)) assessed by trichrome staining. Remarkably, fibrosis area statistically significantly associated with ΔADC_{2w} (R = 0.707, $P < .001$) (Figure 5(e)) and ΔADC_{3w} (R = 0.474, $P = .047$) (Figure 5 (f)).

Intratumor immune responses of the combination of IRE and DC vaccination in KPC tumor

We examined the calreticulin (CRT), one of the hallmarks of immunogenic cell death, in the KPC tumor (Figure 6(a)). The CRT expression, shown as integrated optical density (IOD), was

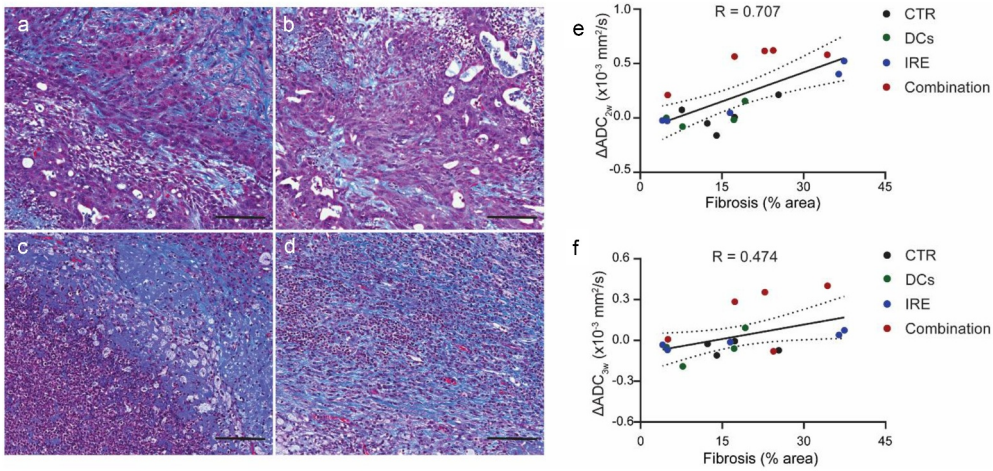

Figure 5. Trichrome staining and quantitative measurement of the fraction of fibrotic area. Representative images of trichrome staining of, (a), control, (b), DC vaccine, (c), IRE treatment, and (d), combination IRE and DC vaccine treatment three weeks after tumor inoculation. Scale bars represent 100 μm. (e), Linear correlation analyses between ΔADC_{2w} values and histology measurement of fibrosis area. R = 0.707, $P < .001$. (f), Linear correlation analyses between ΔADC_{3w} values and histology measurement of fibrosis area. R = 0.474, $P = .047$.

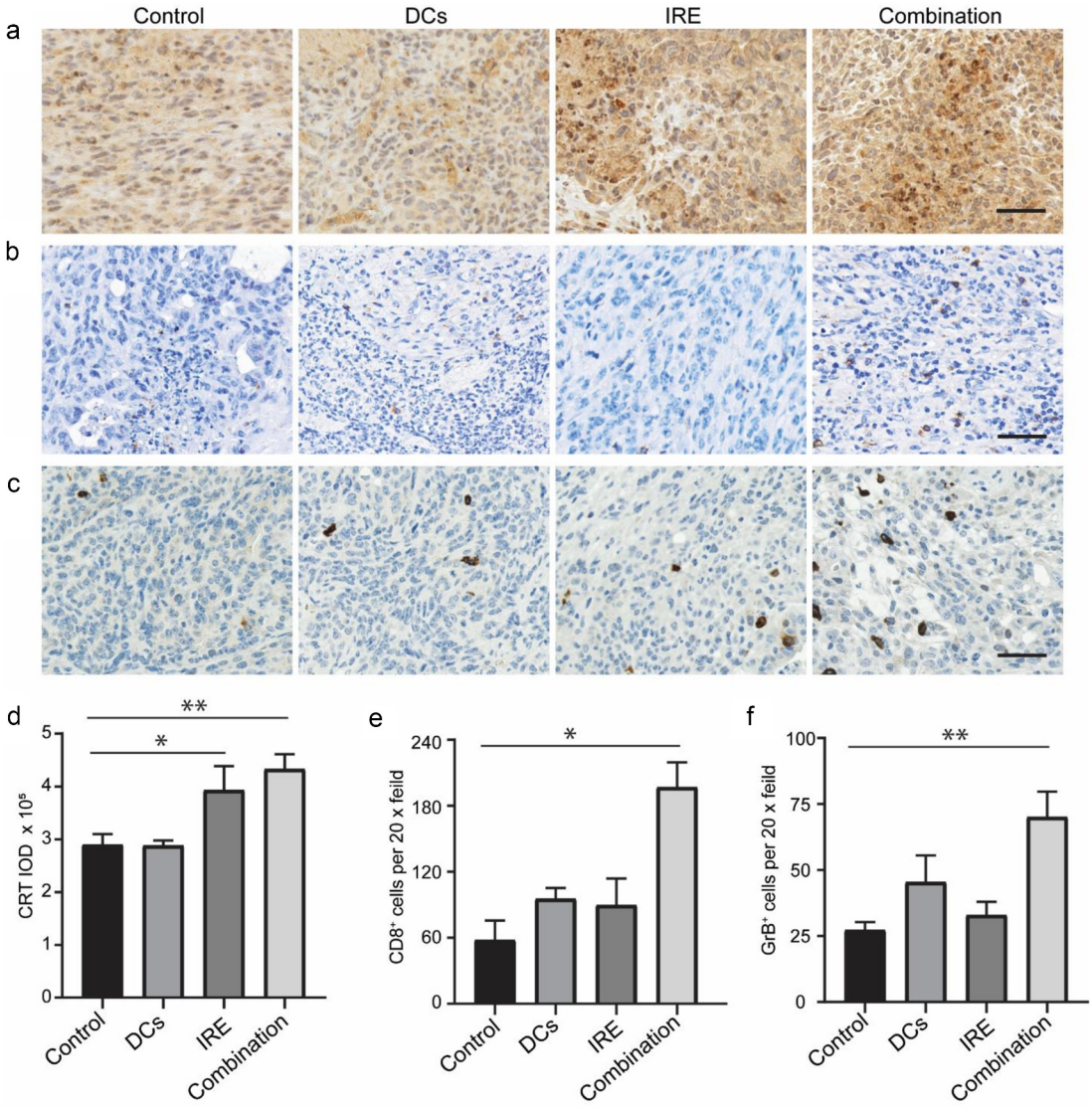

Figure 6. Intratumor immune responses of the combination of IRE and DC vaccination in KPC tumor. Representative images of tumor CRT (a), CD8 (b), and GrB (c) immunostaining after application of different treatments. Scale bars represent 40 μm. Relative quantification of CRT IOD (d), $CD8^+$ (e) cells and GrB^+ (f) in KPC tumors for each group. Data are presented as mean ± SEM, n = 5. *$P < .05$, ** $P < .01$.

upregulated in both IRE treated and combination-treated KPC tumors (Figure 6(d)). Next, we evaluated intratumor infiltrating $CD8^+$ T cells in the KPC tumor (Figure 6(b)). Our results showed that the mean number of $CD8^+$ T cells was higher in the group treated with combination of IRE and DC vaccination than other groups ($P = .001$) (Figure 6(e)). Meanwhile, we assessed the expression of GrB, a granule enzyme expressed by cytotoxic lymphocytes, in the KPC tumors (Figure 6(c)). The mean number of GrB positive cells was significantly higher in combination of IRE and DC vaccination group than control groups ($P = .007$) (figure 6(f)).

Discussion

Our study showed that PDAC IRE ablation alters TME. DW-MRI can capture the changes of tumor fibrosis after IRE ablation. The combined IRE and DC vaccination significantly prolonged the overall survival of immunocompetent mice bearing KPC tumor. The median survival time of KPC tumor-bearing mice for the combined IRE with DC vaccines was 70 days after the initiation of treatment. Moreover, there was a statistically significant difference in the reduction of tumor ADC after the IRE treatment, particularly when combined with the DC vaccines. Furthermore, a strong correlation was observed between the change in tumor ADC and the fibrosis area.

PDAC represents an immune quiescent, so-called "cold" tumor that is particularly poorly infiltrated by $CD8^+$ T cells and thus, is not sensitive to single agent immunotherapy. IRE has remarkable potential for the treatment of advanced PDAC.[18–21] Additionally, IRE procedures inherently induce a release of immunostimulatory cytokines due to nanopore formation. Previous studies have shown that IRE mediates antitumor response to overcome the immunosuppression by modifying TME.[12,14,22] In this study, we combined IRE ablation and DC vaccination to overcome tumor immunosuppression of PDAC. Remarkably, 36% of the mice in combination IRE with DC vaccination group showed tumor eradication. Previous studies reported that IRE can induce the immunogenic cell death of tumor cells by releasing ATP that can regulate the

immunogenicity of tumor.[23,24] Our results also showed that the CRT expression was upregulated in both IRE treated and combination-treated KPC tumors, which further supported that IRE induces immunogenic cell death *in vivo*. Zhao *et al.* showed that IRE treatment boosts the treatment effect of anti-PD1 immunotherapy in KRAS* PDAC tumor by alleviating stroma-induced immunosuppression.[24] Our *in vivo* study showed that the immunosuppressive TME was modulated by IRE or DC vaccines, and more significantly modulated by IRE with DC vaccination, which was demonstrated by increased expression of $CD8^+$ T and GrB^+ cells in PDAC tumors. However, IRE ablation induced obviously increased necrosis size while did not change the stroma fibrosis formation in our study, which can be explained by the robustly basic steps of the "wound healing" process after IRE.[25]

DW-MRI is very sensitive to cell death and tissue damage, particularly during targeted ablation therapies.[26–28] The ADC map generated from DW-MRI reflects molecular diffusion of water within tissue. Vroomen *et al.* reported a tumor ADC increase for the first 24 hours after tumor IRE ablation, followed by a decrease below the pre-treatment values 2 weeks later, and then a return to pre-treatment values as early as 6 weeks later.[7] We also found a transient significant increase of the mean ADC in KPC tumors treated with IRE ablation, particularly combined with the DC vaccination, 1 week after the procedure, and then slightly decrease above the pre-treatment values. Kurosawa *et al.* reported that mean ADC could correlate with tumor fibrosis and cellularity in pancreatic cancer.[29] They also demonstrated that ADC values have the potential to serve as a prognostic marker for patients with resected pancreatic cancer. Wang *et al.* evaluated the mean ADC in PDAC with different stages and reported that PDACs containing dense fibrosis have significantly lower ADC compared to those containing loose fibrosis.[30] Additionally, the change of pre- and post-treatment average ADC values was found to have significant correlation with pathological response in PDAC patients following neoadjuvant chemoradiation treatment.[31] Our results found that the ΔADC_{2w} showed superior linear correlation with histology measurement of fibrosis area when compare with ΔADC_{3w}. To our knowledge, this is the first study that demonstrated that the changes of ADC were strongly correlated with the tumor fibrosis area in PDAC following IRE treatment, which suggested that ADC can be used to early assess treatment response for PDAC.

One limitation of this study was the relatively small sample size in each group for *in vivo* MRI. However, previous studies demonstrated ADC function in IRE tumor ablation and DC vaccination, respectively.[13,32–34] Another limitation was that MRI approaches utilized in this study do not directly describe the effects on tumor cell membrane integrity. Functional MRI techniques to detect tumor cell membrane permeability are needed in this area to further study the effect of combination therapy on tumor cells. In this study, there are no statistically significant differences in tumor growth rate in the first 3 weeks. The tumor volume may not change due to the pseudoprogression during the immune-related treatment. Additional long-term time points for MRI acquisition may provide improved information about tumor volume changes after treatment. Furthermore, combination IRE with DC vaccination has not been tested for treatment PDAC in both preclinical and clinical settings. Further investigations are warranted to refine our results and to undertake the complex signaling mechanism after IRE as well as the interactions among fibrosis, immune cells, and tumor progression.

In conclusion, we found that the ADC values could be used to early assess treatment response for PDAC. We also demonstrated that IRE ablation overcomes tumor-associated immunosuppression to improve the efficacy of DC vaccination by combining it with DC vaccination. Our findings provide a strong rationale for further exploratory testing of combination IRE and DC vaccination in patients with PDAC.

Methods

Cell lines

KPC cells were derived from a transgenic spontaneous tumor in a 6-month-old KPC mouse and used for growing orthotopic tumors in mice and the cellular studies. Cells were cultured on collagen-coated plastic for <12 passages as previously described.[32]

Generation of mature DCs

DCs were derived from bone marrow progenitor cells as described.[32] Briefly, 6–8 weeks old C57BL/6 female mice were used for the generation of DCs. The bone marrow cells were harvested from the femurs. Then, the cells were cultured in complete RPMI1640 containing mouse recombinant IL-4 (1 ng/ml) and GM-CSF (10 ng/ml) (both Invivogen, San Diego, CA) for 8 days in a petri dish. On day 8, immature DCs were harvested by collecting non-adherent cells and then immediately pulsed by incubation with KPC tumor cell lysates in the presence of 100 ng/ml IFN-γ and 250 ng/ml LPS – E. coli 0111:B4 (both from Invivogen, San Diego, CA). KPC lysates were generated by collecting and resuspending KPC tumor cells at 1×10^6 cells/ml in PBS, followed by irradiation with UV for 20 minutes (0.75 J/cm^2) and 24 h incubation.

Orthotopic KPC tumor implantation

All the mice experiments were performed following the protocols approved by our Institutional Animal Care and Use Committee. 8–10 weeks old C57BL/6 female mice (Charles River, Wilmington, MA) were used for establishing orthotopic PDAC models. 5×10^4 viable KPC cells (<12 passages) suspended in a 3:1 PBS to Matrigel (Sigma-Aldrich, St Louis, MO) solution were directly injected into the pancreas for orthotopic tumor induction. Mice were randomly assigned into different groups at 4–5 days following tumor inoculation.

Tumor IRE ablation

For the *in vitro* studies, KPC cells were washed and trypsinized, then resuspended in PBS at 2×10^6 cells/ml. Then, the cells were transferred to a cuvette (Cat#FB104, Thermo Fisher Scientific, Waltham, MA) for electroporation. The cells were

subjected to electroporation with the following parameters, 500 or 1000 V, 1 Hz of pulse repetition frequency, 100 μs pulse duration, and 20 pulses at room temperature. The cell suspension was centrifuged at 4°C, 300 g for 5 min. Supernatants were collected for ATP measurement immediately. The cell pellets were then re-suspended in Annexin V binding buffer and subsequently stained with Annexin V/PI (Cat# 640914, BioLegend, San Diego, CA). The cell suspension was then analyzed by flow cytometry (FACSCalibur; BD Biosciences, San Jose, CA). The data were collected and analyzed using the FlowJo software (TreeStar Inc, Ashland, OR).

The experimental procedure for KPC tumor ablation was conducted as described previously.[35] In brief, IRE was conducted by using the BTX Harvard Apparatus electroporation function generator (ECM830, Holliston, MA). For *in vivo* IRE experiments, KPC tumor-bearing mice were anesthetized by inhalation of isoflurane (1–2% in oxygen, 2 L/min). IRE was performed using a BTX Harvard Apparatus Platinum Tweezertrode, 7 mm diameter (BTX item #45-0488, Holliston, MA). The Tweezertrode was clipped the center of exposed pancreatic cancer nodule along the largest long axis. The electroporation parameters were as follows: 1000 V, 1 Hz of pulse repetition frequency, 100 μs of pulse duration, and 99 pulses. Then, the incision was closed.

Monitoring of tumor growth and therapeutic effects

The experimental setup, MRI scanning and treatment schedule are depicted in Figure 1(a). Orthotopic KPC mice were enrolled after 7 days of tumor inoculation. Tumor IRE ablation was performed on day 8 after tumor inoculation. 3×10^6 DC vaccination was intraperitoneally delivered on day 1, 8, and 15 after enrollment. Thirty-six KPC tumor-bearing mice were used for evaluation of the overall survival. Survival events were recorded when mice displayed >15% loss of total body weight, >1.8 cm tumor diameter, decreased mobility, or per absolute survival event. All mice enrolled in this study were regularly weighed and monitored for signs of pain and stress.

For MRI study, 20 KPC-tumor-bearing mice were equally assigned into four groups for different treatments and were euthanized after the last MRI examination to collect tissue for histology. MRI was performed weekly for three times. Mice were anesthetized by inhalation of isoflurane (1–2% in oxygen, 2 L/min). Experiments were performed with a Bruker 7.0 T MRI scanner with a commercial mouse coil (ClinScan, Bruker Biospin). The pancreas was localized using coronal and axial T2W images (Turbo Spin Echo (TSE); slice thickness (ST): 1.0 mm; Repetition time (TR): 1600 m; Echo time (TE): 37 ms; flip angle (FA): 180°; 1600 ms; field of view (FOV): 36×28 mm^2). The MRI sequences and parameters were as follows: (a) axial T2-weighted imaging: TSE; TR: 2100 ms; ST: 0.5 mm; TE: 40 ms; FA: 180°; FOV: 21×30 mm^2; (b) coronal T2W imaging: TSE; TR: 2100 ms; ST: 0.5 mm; TE: 40 ms; FA: 180; FOV: 40×30 mm^2; (c) axial diffusion-weighted imaging (DW-MRI): Echo Planar Imaging; TR: 2700 ms; ST: 1 mm; TE: 40 ms; FA: 90°; FOV: 24×30 mm^2; b value = 0, and 800 s/mm^2. ITK-SNAP 3.6 (http://www.itksnap.org/pmwiki/pmwiki.php) was used to calculate tumor volumes of the segmented structures. MATLAB R2018a (Mathworks, Natick, MA) and ImageJ 1.52a (http://imagej.nih.gov/ij) were used for additional image processing and ADC calculations. The changes of tumor ADC (ΔADC) were determined according to the equation: $\Delta ADC_{Nw} = ADC_{Nw} - ADC_{1w}$, where ADC_{1w} and ADC_{Nw} are tumor mean ADC calculated at 1 week and N weeks post-tumor inoculation, respectively.

Histology analysis

Pancreatic tumor tissues were fixed in 10% formalin for histologic analysis. Sections of 5 μm were selected for Masson's Trichrome and H&E stains according to the manufacturer's instructions. For immunohistochemistry, 5 μm-thick slides were deparaffinized in xylene and then rehydrated in ethanol. Subsequently, sections were pretreated to antigen retrieval in Citra antigen retrieval solution (Vector, Burlingame, CA) by steam heating. Then, the tissue slides were incubated in blocking buffer (2.5% BSA, 5% goat serum in 1× PBS) for 1 h at room temperature, and thereafter, sections were stained overnight at 4°C with anti-mouse CK19 (kindly provided by the Developmental Studies Hybridoma Bank), rabbit anti-Granzyme B (GrB) antibody (Cat#ab4059, Abcam, Cambridge, MA), and rat monoclonal anti-mouse CD8 (Cat#14-0808-82, Invitrogen, Waltham, MA), rabbit anti-Calreticulin antibody (Cat#ab2907, Abcam, Cambridge, MA), and rabbit monoclonal anti-mouse cleaved caspase 3 (Cat#9664 Cell signaling, Danvers, MA). Immunostaining was developed by using 3,3′-diaminobenzidine (DAB) kit (Vector, Burlingame, CA). All stained slides were scanned on TissueFAXS system. Image analysis and quantification were performed using ImageJ software. We performed scoring in a blinded manner to remove observer bias and analyzed a minimum of four random fields under 200x power magnification for five specimens for each parameter.

Statistical analysis

Data are reported as mean and SEM. The replicate *in vitro* experiments and number of mice is depicted in each figure legend. Statistical significance was either assessed via a one-way ANOVA with Bonferroni post test or unpaired two-tailed Student's t-test. The overall survival was analyzed using the Kaplan-Meier method, and survival difference was assessed using log-rank test. $P < .05$ was considered significant. Statistical analysis was performed using GraphPad Prism software version 8.0 (La Jolla, CA, USA).

Acknowledgments

Z.Z. and J. Y. conceived of and designed the study. All authors contributed to aspects of the data analysis and interpretation and the writing of the manuscript.

Disclosure

The authors declare that the research was conducted in the absence of any commercial or financial relationships that could be construed as a potential conflict of interest.

Funding

This study was supported by the National Cancer Institute under Grant R01CA209886 and R01CA241532; 2019 Harold E. Eisenberg Foundation Scholar Award at the Robert H. Lurie Comprehensive Cancer Center; and SIR Foundation Pilot Grant under Grant PR-0000000012.

References

1. Siegel RL, Miller KD, Jemal A. Cancer statistics, 2019. CA Cancer J Clin. 2019;69:7–34. doi:10.3322/caac.21551.
2. Jemal A, Siegel R, Ward E, Hao Y, Xu J, Thun MJ. Cancer statistics, 2009. CA Cancer J Clin. 2009;59:225–249. doi:10.3322/caac.20006.
3. Palucka K, Banchereau J. Dendritic-cell-based therapeutic cancer vaccines. Immunity. 2013;39:38–48. doi:10.1016/j.immuni.2013.07.004.
4. Palucka K, Banchereau J. Cancer immunotherapy via dendritic cells. Nat Rev Cancer. 2012;12:265–277. doi:10.1038/nrc3258.
5. Davalos RV, Mir LM, Rubinsky B. Tissue ablation with irreversible electroporation. Ann Biomed Eng. 2005;33:223. doi:10.1007/s10439-005-8981-8.
6. Martin RCG, McFarland K, Ellis S, Velanovich V. Irreversible electroporation in locally advanced pancreatic cancer: potential improved overall survival. Ann Surg Oncol. 2013;20:443–449. doi:10.1245/s10434-012-2736-1.
7. Vroomen L, Scheffer HJ, Melenhorst M, Jong MC, Bergh JE, Kuijk CV, Delft FV, Kazemier G and Meijerink MR. MR and CT imaging characteristics and ablation zone volumetry of locally advanced pancreatic cancer treated with irreversible electroporation. Eur Radiol. 2017;27:2521–2531. doi:10.1007/s00330-016-4581-2.
8. Narayanan G, Hosein PJ, Arora G, Barbery KJ, Froud T, Livingstone AS, Franceschi D, Lima CMR and Yrizarry J. Percutaneous irreversible electroporation for downstaging and control of unresectable pancreatic adenocarcinoma. J Vasc Interv Radiol. 2012;23:1613–1621. doi:10.1016/j.jvir.2012.09.012.
9. Kwon D, McFarland K, Velanovich V, Martin RC 2nd. Borderline and locally advanced pancreatic adenocarcinoma margin accentuation with intraoperative irreversible electroporation. Surgery. 2014;156:910–920. doi:10.1016/j.surg.2014.06.058.
10. Mansson C, Brahmstaedt R, Nilsson A, Nygren P, Karlson BM. Percutaneous irreversible electroporation for treatment of locally advanced pancreatic cancer following chemotherapy or radiochemotherapy. Eur J Surg Oncol. 2016;42:1401–1406. doi:10.1016/j.ejso.2016.01.024.
11. Schaft N, Dorrie J, Muller I, Beck V, Baumann S, Schunder T, Kämpgen E and Schuler G. A new way to generate cytolytic tumor-specific T cells: electroporation of RNA coding for a T cell receptor into T lymphocytes. Cancer Immunol Immunother. 2006;55:1132–1141. doi:10.1007/s00262-005-0098-2.
12. White SB, Zhang Z, Chen J, Gogineni VR, Larson AC. Early immunologic response of irreversible electroporation versus cryoablation in a rodent model of pancreatic cancer. J Vasc Interv Radiol. 2018;29:1764–1769. doi:10.1016/j.jvir.2018.07.009.
13. Figini M, Wang X, Lyu T, Su Z, Wang B, Sun C, Shangguan J, Pan L, Zhou K, Ma Q, et al. Diffusion MRI biomarkers predict the outcome of irreversible electroporation in a pancreatic tumor mouse model. Am J Cancer Res. 2018;8:1615–1623.
14. Zhang Z, Li W, Procissi D, Tyler P, Omary RA, Larson AC. Rapid dramatic alterations to the tumor microstructure in pancreatic cancer following irreversible electroporation ablation. Nanomed (Lond). 2014;9:1181–1192. doi:10.2217/nnm.13.72.
15. Bipat S, Phoa SSKS, Delden OMV, Bossuyt PMM, Gouma DJ, Laméris JS and Stoker J. Ultrasonography, computed tomography and magnetic resonance imaging for diagnosis and determining resectability of pancreatic adenocarcinoma. J Comput Assist Tomogr. 2005;29:438–445. doi:10.1097/01.rct.0000164513.23407.b3.
16. Chandarana H, Babb J, Macari M. Signal characteristic and enhancement patterns of pancreatic adenocarcinoma: evaluation with dynamic gadolinium enhanced MRI. Clin Radiol. 2007;62:876–883. doi:10.1016/j.crad.2007.03.005.
17. Butts K, Daniel BL, Chen L, Bouley DM, Wansapura J, Maier SE, Dumoulin C and Watkins R. Diffusion-weighted MRI after cryosurgery of the canine prostate. Magnetic resonance imaging. J Magn Reson Imaging. 2003;17:131–135.
18. Ansari D, Kristoffersson S, Andersson R, Bergenfeldt M. The role of irreversible electroporation (IRE) for locally advanced pancreatic cancer: a systematic review of safety and efficacy. Scand J Gastroenterol. 2017;52:1165–1171. doi:10.1080/00365521.2017.1346705.
19. Tasu JP, Vesselle G, Herpe G, Richer JP, Boucecbi S, Vélasco S, Debeane B, Carretier M and Tougeron D. Irreversible electroporation for locally advanced pancreatic cancer: where do we stand in 2017? Pancreas. 2017;46:283–287. doi:10.1097/mpa.0000000000000793.
20. Huang KW, Yang PC, Pua U, Kim MD, Li SP, Qiu YD, Song TQ and Liang PC. The efficacy of combination of induction chemotherapy and irreversible electroporation ablation for patients with locally advanced pancreatic adenocarcinoma. J Surg Oncol. 2018;118:31–36. doi:10.1002/jso.25110.
21. Okada T, Linguraru MG, Hori M, Summers RM, Tomiyama N, Sato Y. Abdominal multi-organ segmentation from CT images using conditional shape-location and unsupervised intensity priors. Med Image Anal. 2015;26:1–18. doi:10.1016/j.media.2015.06.009.
22. Al-Sakere B, Bernat C, Andre F, Connault E, Opolon P, Davalos RV and Mir LM. A study of the immunological response to tumor ablation with irreversible electroporation. Technol Cancer Res Treat. 2007;6:301–306. doi:10.1177/153303460700600406.
23. Krysko DV, Garg AD, Kaczmarek A, Krysko O, Agostinis P, Vandenabeele P. Immunogenic cell death and DAMPs in cancer therapy. Nat Rev Cancer. 2012;12:860–875. doi:10.1038/nrc3380.
24. Zhao J, Wen X, Tian L, et al. Irreversible electroporation reverses resistance to immune checkpoint blockade in pancreatic cancer. Nat Commun. 2019;10:899. doi:10.1038/s41467-019-08782-1.
25. Bulvik BE, Rozenblum N, Gourevich S, Ahmed M, Andriyanov AV, Galun E and Goldberg SN. Irreversible electroporation versus radiofrequency ablation: A comparison of local and systemic effects in a small-animal model. Radiology. 2016;280:413–424. doi:10.1148/radiol.2015151166.
26. Geschwind JF, Artemov D, Abraham S, Omdal D, Huncharek MS, McGee C, Arepally A, Lambert D, Venbrux AC and Lund GB. Chemoembolization of liver tumor in a rabbit model: assessment of tumor cell death with diffusion-weighted MR imaging and histologic analysis. J Vasc Interv Radiol. 2000;11:1245–1255. doi:10.1016/s1051-0443(07)61299-8.
27. Butts K, Daniel BL, Chen L, Bouley DM, Wansapura J, Maier SE, Dumoulin C and Watkins R. Diffusion-weighted MRI after cryosurgery of the canine prostate. Magnetic resonance imaging. J Magn Reson Imagin. 2003;17:131–135. doi:10.1002/jmri.10227.
28. Jacobs MA, Herskovits EH, Kim HS. Uterine fibroids: diffusion-weighted MR imaging for monitoring therapy with focused ultrasound surgery–preliminary study. Radiolog. 2005;236:196–203. doi:10.1148/radiol.2361040312.
29. Kurosawa J, Tawada K, Mikata R, Ishihara T, Tsuyuguchi T, Saito M, Shimofusa R, Yoshitomi H, Ohtsuka M, Miyazaki M, et al. Prognostic relevance of apparent diffusion coefficient obtained by diffusion-weighted MRI in pancreatic cancer. J Magn Reson Imaging. 2015;42:1532–1537. doi:10.1002/jmri.24939.
30. Wang Y, Chen ZE, Nikolaidis P, McCarthy RJ, Merrick L, Sternick LA, Horowitz JM, Yaghmai V and Miller FH. Diffusion-weighted magnetic resonance imaging of pancreatic adenocarcinomas: association with histopathology and tumor grade. J Magn Reson Imaging. 2011;33:136–142. doi:10.1002/jmri.22414.
31. Dalah E, Erickson B, Oshima K,Schott D, Hall WA, Paulson E, Tai A, Knechtges P and Li XA. Correlation of ADC with pathological treatment response for radiation therapy of pancreatic cancer. Transl Oncol. 2018;11:391–398. doi:10.1016/j.tranon.2018.01.018.

32. Yang J, Hu S, Shangguan J, Eresen A, Li Y, Pan L, Ma Q, Velichko Y, Wang J, Hu C, et al. Dendritic cell immunotherapy induces anti-tumor effect in a transgenic mouse model of pancreatic ductal adenocarcinoma. Am J Cancer Res. 2019;9:2456–2468.
33. Pan L, Shang N, Shangguan J, Figini M, Xing W, Wang B , Sun C, Yang J, Zhang Y, Hu S, et al. Magnetic resonance imaging monitoring therapeutic response to dendritic cell vaccine in murine orthotopic pancreatic cancer models. Am J Cancer Res. 2019;9:562–573.
34. Shangguan A, Shang N, Figini M, Pan L, Yang J, Ma Q, Hu S, Eresen A, Sun C, Wang B, et al. Prophylactic dendritic cell vaccination controls pancreatic cancer growth in a mouse model. Cytotherapy. 2020;22:6–15. doi:10.1016/j.jcyt.2019.12.001.
35. Cemazar M, Sersa G, Frey W, Miklavcic D, Teissié J. Recommendations and requirements for reporting on applications of electric pulse delivery for electroporation of biological samples. Bioelectrochemistry. 2018;122:69–76. doi:10.1016/j.bioelechem.2018.03.005.